Experimental investigation of obstacle-aided locomotion with a snake robot

Pål Liljebäck, *Member, IEEE,*
Kristin Y. Pettersen, *Senior Member, IEEE,*
Øyvind Stavdahl, *Member, IEEE,*
and Jan Tommy Gravdahl, *Senior Member, IEEE*

Abstract—In a recent work, the authors have proposed a control strategy for a snake robot during *obstacle-aided locomotion*. In the present work, experimental results are presented where the controller is shown to successfully maintain the forward propulsion of a physical snake robot in a course with different obstacle configurations.

Index Terms—Snake robot, Underactuated Robots, Force and Tactile Sensing, Contact Modelling.

I. INTRODUCTION

Inspired by biological snake locomotion, snake robots carry the potential of meeting the growing need for robotic mobility in unknown and challenging environments. These mechanisms typically consist of serially connected joint modules capable of bending in one or more planes. The many degrees of freedom of snake robots make them difficult to control, but provide traversability in irregular environments that surpasses the mobility of the more conventional wheeled, tracked and legged forms of robotic mobility.

A unique feature of snake robot locomotion compared to other forms of robotic mobility is that ground irregularities are beneficial for the propulsion since they provide push-points for the robot. These ideas are in line with early work by Gray [1], who concluded that forward motion of a planar snake requires the existence of external forces acting in the normal direction of the snake body, and also the work in [2], which studies the motion of biological snakes as they interact with pegs in order to push themselves forward. While *obstacle avoidance* is important for wheeled, tracked and legged robots, the goal of snake locomotion is rather *obstacle exploitation*. The term *obstacle-aided locomotion* was introduced by Transeth *et al.* [3] and captures the essence of this concept.

The majority of previous research on *control* of snake robots has focused on open-loop strategies for flat surface motion aimed at resembling gaits displayed by biological snakes (see e.g. [4]–[10]). Only a few works present control strategies related to obstacle-aided snake locomotion (i.e. where the surface is no longer assumed to be flat). Hirose [11] studied biological snakes and proposed a strategy for *lateral inhibition* that modifies the shape of a snake robot based on contact force sensing along the snake body in order to *avoid* obstacles. The work in [12] proposes an inverse dynamics approach by formulating and numerically solving an optimization problem in order to, for a given set of obstacle contacts, calculate the contact forces required to propel the snake in a desired direction. A strategy for calculating the actual torque inputs to the joints from the desired contacts is, however, not presented. A kinematic approach is proposed in [13], where a curve fitting procedure is used to determine the shape of the snake with respect to the obstacles. Subsequently, this shape is propagated backwards along the snake body under the assumption that this will push the robot forward. Along with these works, we should also mention the work in [14], which analyses how obstacles around a snake robot affect its degrees of freedom.

Sensing the environment of a snake robot must not necessarily involve contact force sensing since the environment can be indirectly

sensed through the joint angle measurements and/or the actuator torques. This approach is considered in [15], where the joint torques of a snake robot are specified solely in terms of the measured joint angles to achieve motion through a winding corridor, and in [16], which presents a control strategy that uses motor current measurements to adjust the shape of a snake robot moving through an elastically deformable channel, and in [17], where the deviations of the joint angles from their setpoints are used to adapt the body shape of a snake robot moving inside pipe structures.

In [18], we have proposed a control law for obstacle-aided locomotion aimed at resolving situations where the snake robot is jammed between obstacles. The controller employs feedback of measured contact forces along the body of the snake robot to maintain the propulsion. In this paper, *experimental results* are presented where the controller proposed in [18] is implemented on a physical snake robot placed in a course with different obstacle configurations that are not known to the robot. The experiments show that the proposed controller successfully maintains the forward propulsion of the snake robot during the interaction with the obstacles and enables the robot to move through all the considered obstacle courses. Quite few experimental results on obstacle-aided locomotion have been reported. The objective of this paper is to bridge the gap between theory and practice and hopefully contribute to the continued pursuit of general control strategies for intelligent and adaptive snake robot locomotion.

The paper is organized as follows. Section II summarizes a mathematical model of a snake robot in an environment with obstacles. Section III presents the control strategy for obstacle-aided locomotion. Section IV presents the experimental results that illustrate the performance of the controller. Finally, Section V presents concluding remarks.

II. THE MODEL OF THE SNAKE ROBOT

This section summarizes a hybrid model of the dynamics of a snake robot interacting with obstacles. The main purpose of the section is to introduce the notation that will be employed in the presentation of the controller in Section III. For a more detailed presentation of the model, the reader is referred to [18].

The snake robot is illustrated in Fig. 1(a) and consists of n links of length $2l$ interconnected by $n-1$ joints. All n links have the same mass m and moment of intertia $J = \frac{1}{3}ml^2$. The snake robot moves in the horizontal plane and has $n+2$ degrees of freedom. The position of the CM (center of mass) of the robot is denoted by $p = (p_x, p_y)$. The absolute angle θ_i of link i (i.e. the orientation of link i) is expressed with respect to the global x axis with counterclockwise positive direction. As seen in Fig. 1(a), the relative angle between link i and link $i+1$ (i.e. the joint angle of joint i) is given by

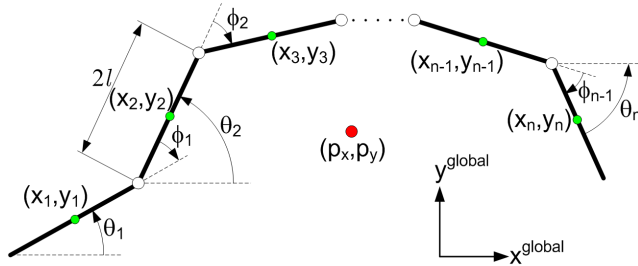$$\phi_i = \theta_i - \theta_{i+1}. \tag{1}$$

The forces and torques acting on a link that is not in contact with an obstacle are shown in Fig. 1(b). The forces $h_{x,i}$ and $h_{y,i}$ are constraint forces that hold joint i together. The actuator torque at joint i is given by u_i. The isotropic Coulomb ground friction force on link i, denoted by $f_{R,i}$, acts on the CM of the link and the friction torque, $\tau_{R,i}$, acts about the link CM. The ground friction coefficient is denoted by μ.

The planar environment of the snake robot consists of an arbitrary number of external obstacles with circular shape. The interaction between a snake robot link and an obstacle is modelled by introducing a *unilateral velocity constraint* for the link when it comes into contact with an obstacle. The constraint is *unilateral* (acts in one lateral direction only) since the constraint shall allow sideways motion of the link *away* from the obstacle, but prevent any sideways motion *towards* (and thereby into) the obstacle. As illustrated in Fig. 1(c), the obstacle contact force on link i is assumed to act on the CM of the link and consists of two orthogonal components. The first component is the *constraint force*, $f_{c,i}$, acting in the normal direction of link i
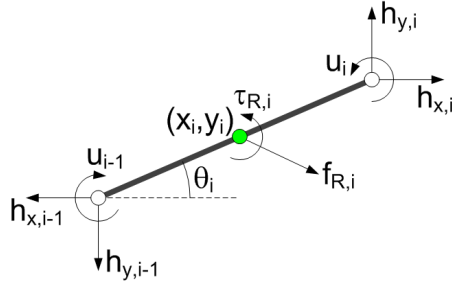
(a) The kinematic parameters of the snake robot.

(b) Forces and torques acting on a link that is not in contact with an obstacle.
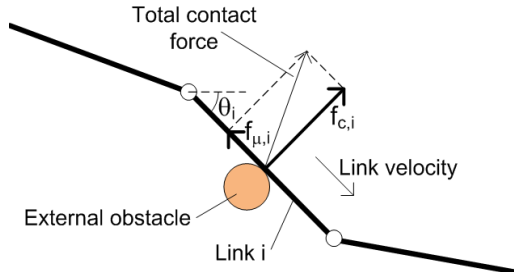
(c) The obstacle contact force on a link consisting of the normal direction constraint force and the tangential direction friction force.

Fig. 1. Parameters that define the kinematics and dynamics of the snake robot.

and away from the obstacle. The second component is the obstacle *friction force*, $f_{\mu,i}$, acting in the tangential direction of link i and in the opposite direction of the tangential link velocity. The friction coefficient between the snake robot and any obstacle is denoted by μ_o.

The model of the snake robot is developed within the framework of a *hybrid dynamical system* [19] to handle the discontinuous nature of the model, i.e. to ensure that obstacle contact forces only occur when a link comes into contact with an obstacle. It is shown in [18] that the complete model can be written as

$$
\begin{aligned}
\dot{x} &= F(x, u) \quad \text{for all} \quad x \in C, \\
x^+ &= G(x) \quad \text{for all} \quad x \in D,
\end{aligned}
\tag{2}
$$

where x is the state vector and u is the vector of joint actuator torques. The state vector x flows continuously according to the *flow map* F as long as the state belongs to the *flow set* C, which is the set of all states where the set of links that are in contact with obstacles remains fixed. The state vector enters the *jump set* D when a link impacts or detaches from an obstacle. In this case, the state will experience a jump according to the *jump map* G. During an impact, the jump map basically cancels the normal direction velocity of the impacted link to prevent it from continuing into the obstacle.

III. THE CONTROLLER FOR OBSTACLE-AIDED LOCOMOTION

This section presents the control strategy for obstacle-aided locomotion which is experimentally investigated in Section IV. The controller represents a hybrid system since it contains timers and logic state values. In [18], the controller is therefore formulated within the hybrid modelling framework employed for the model of the snake robot in the previous section. Due to space restrictions, this section only gives an informal description of the controller without considering the hybrid modelling framework.

A. Overview of the control strategy

A major challenge during obstacle-aided locomotion is to prevent the snake robot from being *jammed* between the obstacles. In a jammed situation, the *propulsive* components (i.e. the force components in the desired direction of motion) of the contact forces from the obstacles are too small to overcome the friction forces on the robot, and hence the forward motion stops.

The control strategy proposed in the following is a *hybrid controller* consisting of a *leader-follower* scheme and a *jam resolution* scheme, and also a supervisory mechanism for switching between these two schemes, denoted the *jam detection* scheme. The *leader-follower* scheme is carried out as long as the robot is able to move without being jammed between the obstacles. If the *jam detection* scheme detects a jam, the *jam resolution* scheme is carried out in order to effectively 'unlock' the jammed joints. The hybrid controller produces the torque input vector, $u \in \mathbb{R}^{n-1}$, for the $n-1$ joints of the robot. We assume that the link angles, $\theta \in \mathbb{R}^n$, the link angle velocities, $\dot{\theta} \in \mathbb{R}^n$, and the constraint forces, $f_c \in \mathbb{R}^n$, are measured.

Note that the following control strategy is not intended as a complete motion controller for propelling a snake robot through an arbitrary environment. An important limitation of the control strategy is the underlying assumption that there are sufficiently many obstacles in reach of the snake robot. Without obstacles, there are no push-points that the robot can use for propulsion. At the same time, the control strategy will not work if there are too many obstacles so that the path of the robot is blocked. These are not critical issues, however, since the main purpose of the controller is simply to demonstrate how a snake robot can utilize contact forces from objects in its environment to achieve propulsion. There are several aspects of the control strategy that must be addressed in order to achieve obstacle-aided locomotion in more general environments. For instance, the control strategy assumes that the snake robot moves on a horizontal surface with vertical obstacles, which is not a valid assumption for snake robot locomotion in general.

B. The leader-follower scheme

The leader-follower scheme is motivated by the fact that each part of a biological snake conducting lateral undulation follows the path traced out by the head [1]. We therefore choose the head joint angle (the foremost joint), ϕ_{n-1}, as the reference angle for all subsequent joints. The preferred direction of motion for the snake is defined to be along the global positive x axis.

In order to achieve the sinusoidal motion characteristic of lateral undulation, we alternate between moving the head in the leftward and rightward direction with respect to the global positive x axis. As illustrated in Fig. 2, this may be achieved by choosing the reference angle for the head link, $\theta_{n,\text{ref}}$, according to the rule

$$
\begin{array}{llll}
\text{Leftward motion:} & \theta_{n,\text{ref}} = \theta_{\text{left}} & \text{until} & \Delta y > \Delta y_{\text{max}}, \\
\text{Rightward motion:} & \theta_{n,\text{ref}} = \theta_{\text{right}} & \text{until} & \Delta y < -\Delta y_{\text{max}},
\end{array}
\tag{3}
$$

where $\theta_{\text{left}} > 0$ and $\theta_{\text{right}} < 0$ are design parameters, $\triangle y$ is the distance between the head position and the CM position of the snake robot along the global y axis, and $\triangle y_{\text{max}}$ is the predefined amplitude of the head motion perpendicular to the direction of locomotion. To
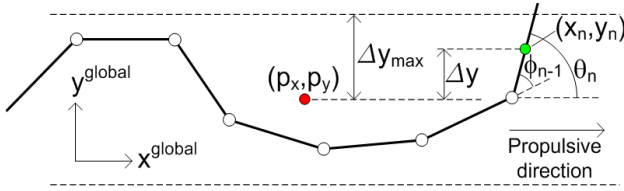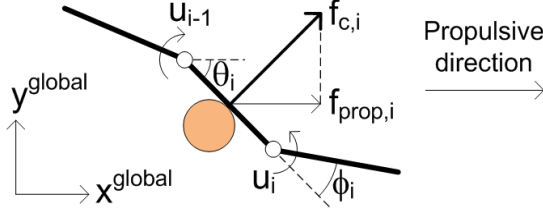
Fig. 2. Control of the head of the snake robot.

Fig. 3. The propulsive component, $f_{\mathrm{prop},i}$, of the constraint force on link i.

obtain the head *link* angle, the head *joint* angle, ϕ_{n-1}, is controlled according to the reference

$$\phi_{n-1,\mathrm{ref}} = \theta_{n-1} - \theta_{n,\mathrm{ref}}. \tag{4}$$

The head joint angle is propagated backwards along the snake body at a predefined velocity, v_{ref}, and used as the reference angle for all subsequent joints. For a given choice of v_{ref}, the time offset, $\triangle t$, between two consecutive joints with intermediate distance $2l$ is found as $\triangle t = \frac{2l}{v_{\mathrm{ref}}}$.

To summarize, the reference angles for all the joints of the snake robot in this leader-follower scheme are

$$\begin{aligned} \phi_{n-1,\mathrm{ref}}(t) &= \theta_{n-1}(t) - \theta_{n,\mathrm{ref}}, \\ \phi_{i,\mathrm{ref}}(t) &= \phi_{n-1}(t-(n-i-1)\triangle t) \quad \forall \ i = 1, \cdots, n-2. \end{aligned} \tag{5}$$

The design parameters θ_{left}, θ_{right}, $\triangle y_{\max}$, and v_{ref} were introduced in order to calculate these reference angles.

C. The jam detection scheme

A single joint of the snake robot is defined to be *jammed* if the deviation between the joint angle and its reference angle exceeds a certain limit, $\triangle \phi_{\max}$. The entire snake robot is defined to be *jammed* if two or more joints are jammed, which occur when the contact forces cause two or more joints to act 'against' each other. If the robot is jammed over a continuous period longer than $t_{\mathrm{jam,max}}$, the leader-follower scheme is stopped in order to carry out the jam resolution scheme. We let the robot execute jam resolution for a predefined amount of time, $t_{\mathrm{resolution,max}}$, since there is currently no criterion for detecting that the jam has been resolved. Subsequently, the leader-follower scheme continues.

In summary, the design parameters $\triangle \phi_{\max}$, $t_{\mathrm{jam,max}}$, and $t_{\mathrm{resolution,max}}$ determine the switching between the *leader-follower* scheme and the *jam resolution* scheme.

D. The jam resolution scheme

In the jam resolution scheme, the links affected by contact forces are rotated so that the *propulsive component* of each contact force increases. By *propulsive component*, we mean the force component in the desired direction of motion. Rotating the contacted links to increase the total propulsive contact force should resolve a jammed situation.

The measured constraint force on link i is denoted by $\hat{f}_{c,i} \in \mathbb{R}$ and represents the magnitude of the constraint force vector, $f_{c,i} \in \mathbb{R}^2$. The propulsive component, $\hat{f}_{\mathrm{prop},i} \in \mathbb{R}$, of the constraint force on

link i is illustrated in Fig. 3 and is defined as the force component along the global positive x axis, i.e. as

$$\hat{f}_{\mathrm{prop},i} = -\hat{f}_{c,i} \sin \theta_i. \tag{6}$$

The change of the propulsive force due to a change of the link angle is found by differentiating (6) with respect to θ_i:

$$\frac{\partial \hat{f}_{\mathrm{prop},i}}{\partial \theta_i} = -\hat{f}_{c,i} \cos \theta_i. \tag{7}$$

During jam resolution, we choose to rotate links with a high propulsive force gradient with respect to the link angle, which suggests that link i is rotated according to

$$\triangle \theta_{i,\mathrm{ref}} = k_\theta \frac{\partial \hat{f}_{\mathrm{prop},i}}{\partial \theta_i} = -k_\theta \hat{f}_{c,i} \cos \theta_i, \tag{8}$$

where k_θ is a controller gain. We choose to change only the angle of link i while leaving the angle of link $i-1$ and $i+1$ unchanged. This means that $\triangle \theta_{i-1,\mathrm{ref}} = \triangle \theta_{i+1,\mathrm{ref}} = 0$. From the relation $\phi_i = \theta_i - \theta_{i+1}$, we may now write the desired change of the joint angles at each side of link i as

$$\begin{aligned} \triangle \phi_{i-1,\mathrm{ref}} &= \triangle \theta_{i-1,\mathrm{ref}} - \triangle \theta_{i,\mathrm{ref}} = k_\theta \hat{f}_{c,i} \cos \theta_i, \\ \triangle \phi_{i,\mathrm{ref}} &= \triangle \theta_{i,\mathrm{ref}} - \triangle \theta_{i+1,\mathrm{ref}} = -k_\theta \hat{f}_{c,i} \cos \theta_i. \end{aligned} \tag{9}$$

We choose to leave the head joint angle, ϕ_{n-1}, unchanged to avoid that any jam resolution motion of the head link propagates backwards to all other links once the leader-follower scheme resumes. Furthermore, we use the constraint forces that were measured at the instant the jam resolution scheme was initiated, denoted by $f_{\mathrm{jam}} \in \mathbb{R}^n$, as a *constant* feedback during jam resolution, i.e. we do not update the force measurements *during* jam resolution. This ensures a steady rotation of the contacted links in accordance with the contact forces that produced the jam. From the above discussion, the reference angles for all the joints of the snake robot in the jam resolution state may now be summarized as

$$\begin{aligned} \phi_{n-1,\mathrm{ref}} &= \phi_{n-1}, \\ \phi_{i,\mathrm{ref}} &= \phi_i + k_\theta \left(-f_{\mathrm{jam},i} \cos \theta_i + f_{\mathrm{jam},i+1} \cos \theta_{i+1} \right), \end{aligned} \tag{10}$$

where $i \in \{1, \cdots, n-2\}$ and k_θ is a design parameter.

E. Low-level joint angle controller

The joint actuator torques, $u \in \mathbb{R}^{n-1}$, are calculated from the joint reference angles, $\phi_{\mathrm{ref}} \in \mathbb{R}^{n-1}$, according to the PD-controller

$$u = k_P \left(\phi_{\mathrm{ref}} - \phi \right) - k_D \dot{\phi}, \tag{11}$$

where k_P and k_D are the controller gains.

Remark 1: Compliance is an important issue during control based on force feedback. However, there is no need to explicitly consider compliance for the proposed control strategy since we do not attempt to explicitly control the contact forces on the snake robot. Note that the proportional action of the joint torque controller in (11) introduces compliance in the system when the joints are back-drivable since the dynamic properties of a proportional controller are similar to those of a mechanical spring.

IV. EXPERIMENTAL STUDY

This section presents results from an experimental investigation of the control strategy described in Section III.
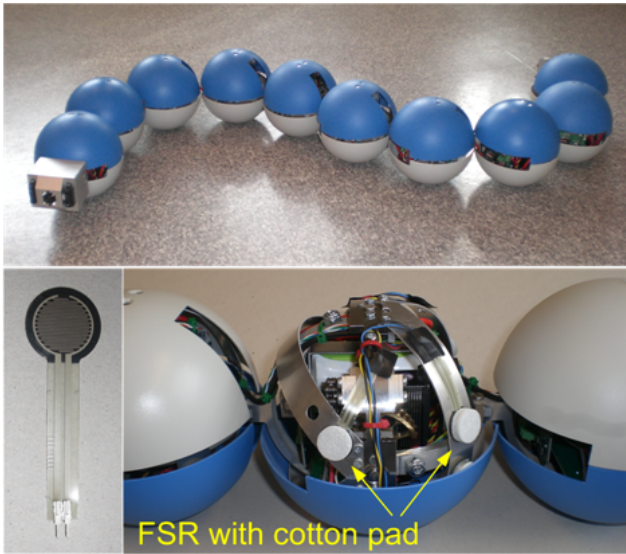
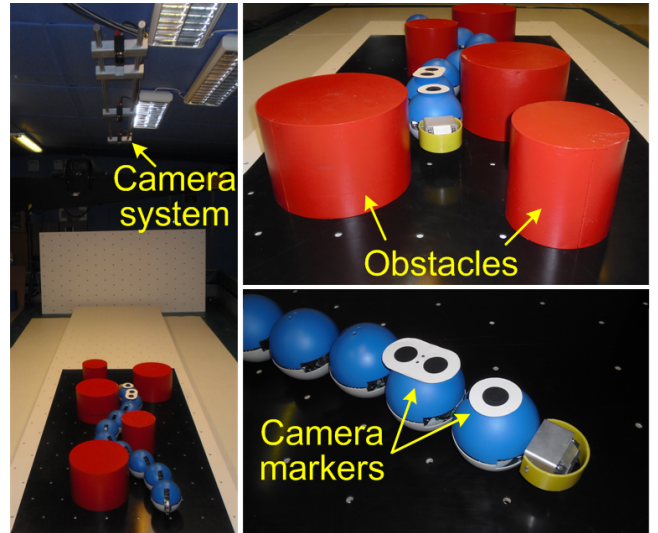Fig. 4. Top: The snake robot used in the experiment. Bottom: The contact force sensor system of the robot.

Fig. 5. The experimental setup. Three cameras mounted in the ceiling measured the position of the snake robot in a course with obstacles. Black markers were mounted on the robot to allow its position to be tracked by SwisTrack.

A. The snake robot

The snake robot used in the experiments is shown in the top of Fig. 4 and described in detail in [20]. The snake robot consists of 10 identical battery-powered joint modules. Each joint module has outer diameter 140 mm, weighs 960 g, and has 2 degrees of freedom (pitch and yaw motion). The maximum joint torque is about 4 Nm and the maximum joint angle is $\pm 45°$.

Each joint module is covered by two hemispherical shells in order to give the robot a smooth outer surface, which is important to achieve gliding locomotion in irregular environments. The ground friction forces acting on the robot are isotropic. Four force sensing resistors (FSRs), two of which are shown in the bottom of Fig. 4, are mounted underneath the shells at each side of a joint module in order to measure the horizontal contact forces from external obstacles. An experimental investigation presented in [20] suggests that the accuracy and performance of the contact force sensor system is adequate for implementing locomotion controllers based on force feedback.

B. Implementation of the obstacle-aided locomotion controller

The hybrid controller described in Section III was implemented on an external computer with the parameters $n = 10$, $l = 0.07$ m, $\theta_{\text{left}} = 50°$, $\theta_{\text{right}} = -50°$, $\Delta y_{\max} = 14$ cm, $v_{\text{ref}} = 5$ cm/s, $\Delta \phi_{\max} = 20°$, $t_{\text{jam,max}} = 1$ s, $t_{\text{resolution,max}} = 1$ s, and $k_\theta = 0.05$. The joint reference angles were sent to the robot through a wireless connection based on Bluetooth at 20 Hz. The joint torque controller given by (11) was not implemented since accurate torque control is not supported by the servo motors installed in the snake robot. The joint angles were instead controlled according to a proportional controller implemented in the microcontroller of each joint module.

C. The setup of the experiment

The snake robot was placed on a black horizontal surface measuring about 100 cm in width and 200 cm in length. As shown in Fig. 5, circular obstacles were placed around the robot. The location of each obstacle could easily be changed by means of a grid of mounting holes in the floor. The purpose of the experiments was to show that the snake robot described in Section IV-A is propelled through several different obstacle courses when the robot is controlled according to the control strategy presented in Section III.

The global frame position, x_n and y_n, and the angle, θ_n, of the head link of the snake robot were determined with the open source camera tracking software *SwisTrack* [21]. SwisTrack was configured to track black circular markers (40 mm in diameter) on the snake robot (see the right part of Fig. 5) at 15 frames per second from three firewire cameras (Unibrain Fire-i 520c) mounted in the ceiling (see the left part of Fig. 5). The use of multiple cameras allowed for position measurements over a greater distance than the area covered by a single camera. The cameras were mounted facing downwards approximately 200 cm above the floor and 132 cm apart. SwisTrack estimated the maximum position error to be about 2.1 cm and the average position error to be about 0.6 cm. The global x axis was configured to be parallel to the long side of the course.

Three different obstacle environments were considered. The first obstacle environment contained five obstacles with x coordinates $(-123.9, -89.6, -48.4, -8.2, -0.6)$ cm, y coordinates $(20.2, -15.7, 13.2, -23.5, 24.8)$ cm, and diameters $(30, 20, 30, 30, 20)$ cm, respectively. The second obstacle environment contained four obstacles with x coordinates $(-90.9, -35.5, 5.1, 31.7)$ cm, y coordinates $(-20.3, 4.2, -28.9, 15.9)$ cm, and diameters $(30, 30, 30, 30)$ cm, respectively. The third and final obstacle environment contained four obstacles with x coordinates $(-93.1, -79.4, -17.4, 14.6)$ cm, y coordinates $(-61.7, -6.3, -18.9, 24.3)$ cm, and diameters $(30, 30, 30, 30)$ cm, respectively.

Three trials were carried out in each obstacle environment. The initial link angles in the first, second, and third environment were approximately $\boldsymbol{\theta} = [49°, 43°, 6°, 14°, -19°, -20°, -3°, 16°, 11°, 1°]^T$, $\boldsymbol{\theta} = [58°, 47°, 25°, -14°, -35°, -27°, -12°, 3°, 28°, 25°]^T$, and $\boldsymbol{\theta} = [-4°, -4°, -2°, 15°, 30°, 65°, 40°, 29°, -3°, -22°]^T$, respectively. The initial position of the head link was $(x_N = 0, y_N = 0)$ and the initial reference angle for the head link was $\theta_{N,\text{ref}} = \theta_{\text{right}}$ in all three environments.

D. Experimental results

As explained in Section IV-C, the purpose of the experiments was to show that the snake robot described in Section IV-A is propelled through three different obstacle courses when the robot is controlled according to the proposed control strategy. The experimental results from the three obstacle environments are shown in Figures 6 and 7, Figures 8 and 9, and Figures 10 and 11, respectively.

Three trials were carried out in each obstacle environment. The measured position of the head link along the forward direction (the global x axis) during the three trials in each environment are shown in Figures 6(a), 8(a), and 10(a), respectively, and the control scheme executed during each trial (i.e. *leader-following* or *jam resolution*) is shown in Figures 6(b), 8(b), and 10(b). Furthermore, the sideways position (along the global y axis) and the orientation of the head link are shown in Figures 6(c)-(d), 8(c)-(d), and 10(c)-(d). In order to give an idea of the forces needed to propel the robot forward, the measured contact forces on joint modules 3 - 8 (module 1 is the tail) during the first trial in each environment are shown in Figures 6(e)-(f), 8(e)-(f), and 10(e)-(f), respectively. The motion of the snake robot during the first trial in each environment is visualized in Figures 7, 9, and 11, respectively.

As seen by the plots of the head position along the forward direction in Figures 6(a), 8(a), and 10(a), the overall forward propulsion of the snake robot was maintained throughout the trials in all three environments. This was also the main goal of the experiments. In other words, using the same controller with the same set of controller parameters, the snake robot was able to move through three different obstacle environments. The plots of the sideways position and orientation of the head link suggest that the reference angles from the leader-follower scheme were rather different in the individual trials in each environment. However, there is a fairly good repeatability in the forward direction plots from the trials in each environment, which is indicative of the robustness and environment adaptability properties of the proposed controller.

The forward direction plots show that the forward speed of the robot was relatively slow in all trials. This limited speed was due to the limited torque of the joints of the snake robot compared to the rather large ground and obstacle friction forces opposing the motion. In particular, the snake robot is rather heavy (about 10 kg) compared to its maximum actuator torque (about 4 Nm). To cope with the limited strength of the physical snake robot, the propagation velocity of the head joint angle in the leader-follower scheme was set to a rather small value during the experiments, namely $v_{\text{ref}} = 5$ cm/s. Since v_{ref} determines the propagation velocity of the body waves produced during the locomotion, a small value of v_{ref} will naturally lead to a small forward speed of the robot. In other words, we claim that the limited speed during the experiments was caused by limitations of the physical snake robot, and is not a general property of the proposed control strategy. Had the experiments been carried out using a snake robot with a larger actuator strength to weight ratio, then the controller parameters could have been adjusted to increase the forward speed significantly.

There is a clear tendency in the forward direction plots from all three environments that the forward velocity of the robot starts to decrease after about 50 s. The reason for this decrease in velocity is seen from the visualizations in Figures 7, 9, and 11, which show that the robot used about 50 s to pass through each obstacle course. Since the flat surface outside the obstacle courses contained no push-points that the robot could use for propulsion, the forward velocity decreased as the robot moved out of each obstacle course. The proposed control strategy is, in other words, dependent on external objects in order to propel a snake robot with isotropic ground friction properties forward.

As seen in Figures 6(b), 8(b), and 10(b), the snake robot was jammed and executed jam resolution several times during each trial. In order to visualize the behaviour of the snake robot during jam resolution, Fig. 12 shows the snake robot in the first obstacle environment at two time instants when it was jammed ($t = 6$ s and $t = 21$ s) and after jam resolution had been carried out ($t = 7$ s and $t = 22$ s). It is clearly seen from the figure that the jam resolution scheme increased the angles of the jammed joints with respect to the forward direction, thereby increasing the propulsive components of the subsequent obstacle contact forces at these locations. This behaviour is also the intended purpose of the jam resolution scheme, as described in Section III-D.

The high number of jams that occurred during the trials in the three obstacle environments is an interesting observation since it suggests that the *jam* state of the snake robot should be treated as a *continuous* rather than a discrete state. Furthermore, the high number of jams suggests that leader-following should not be conducted in open-loop, but rather combined with continuous use of the measured contact forces. In particular, the jam resolution scheme was active a large number of times during the experiments because the leader-follower scheme did not consider the environment interaction, which caused the robot to become jammed over and over. In future work, the authors will therefore pursue the development of continuous controllers for obstacle-aided locomotion where jam resolution is a continuous action that is performed in parallel with the cyclic wave motion of the snake robot.

In summary, the experimental results indicate that the proposed control strategy is robust with respect to maintaining the overall forward propulsion of a snake robot in various obstacle environments. The ability of the robot to resolve jams clearly suggests that rotating links in contact with obstacles to increase the propulsive force on the robot is a control principle that should be pursued in further work on obstacle-aided locomotion.

V. CONCLUSION

This paper has presented experimental results in order to investigate the effectiveness of the controller for obstacle-aided snake robot locomotion proposed in [18]. The controller, which uses measured contact forces along the snake body to maintain propulsion, was implemented on a physical snake robot placed in a course with different obstacle configurations. The experiments showed that the proposed controller successfully maintained the overall forward propulsion of the robot in all the considered obstacle courses, which supports the underlying control principle of rotating contacted links in order to increase the propulsive force on the snake robot.

The experimental results have inspired the authors to, in future work, pursue the development of continuous controllers for obstacle-aided locomotion where jam resolution is a continuous action that is performed in parallel with the cyclic wave motion of the snake robot.

REFERENCES

[1] J. Gray, "The mechanism of locomotion in snakes," *J. Exp. Biol.*, vol. 23, no. 2, pp. 101–120, 1946.

[2] B. Moon and C. Gans, "Kinematics, muscular activity and propulsion in gopher snakes," *Journal of Experimental Biology*, vol. 201, pp. 2669–2684, 1998.

[3] A. A. Transeth, R. I. Leine, C. Glocker, K. Y. Pettersen, and P. Liljebäck, "Snake robot obstacle aided locomotion: Modeling, simulations, and experiments," *IEEE Trans. Robot.*, vol. 24, no. 1, pp. 88–104, February 2008.

[4] J. Ostrowski and J. Burdick, "Gait kinematics for a serpentine robot," in *Proc. IEEE Int. Conf. Robotics and Automation*, vol. 2, April 1996, pp. 1294–1299.

[5] K. J. Dowling, "Limbless locomotion. learning to crawl with a snake robot," Ph.D. dissertation, Carnegie Mellon University, December 1997.

[6] S. Ma, "Analysis of creeping locomotion of a snake-like robot," *Adv. Robotics*, vol. 15, no. 2, pp. 205–224, 2001.

[7] M. Saito, M. Fukaya, and T. Iwasaki, "Serpentine locomotion with robotic snakes," *IEEE Contr. Syst. Mag.*, vol. 22, no. 1, pp. 64–81, February 2002.

[8] C. Ye, S. Ma, B. Li, and Y. Wang, "Turning and side motion of snake-like robot," in *Proc. IEEE Int. Conf. Robotics and Automation*, vol. 5, 2004, pp. 5075–5080.

[9] F. Chernousko, "Modelling of snake-like locomotion," *Appl. Math. Comput.*, vol. 164, no. 2, pp. 415–434, May 2005.

[10] J. Gonzalez-Gomez, H. Zhang, and E. Boemo, *Locomotion Principles of 1D Topology Pitch and Pitch-Yaw-Connecting Modular Robots*. Advanced Robotics Systems International and I-Tech Education and Publishing, September 2007, ch. 24, pp. 403–428.

[11] S. Hirose, *Biologically Inspired Robots: Snake-Like Locomotors and Manipulators*. Oxford: Oxford University Press, 1993.

[12] Z. Bayraktaroglu and P. Blazevic, "Understanding snakelike locomotion through a novel push-point approach," *J. Dyn. Syst. - Trans. ASME*, vol. 127, no. 1, pp. 146–152, March 2005.

(a) The forward motion of the head.

(b) The executed control scheme.

(c) The sideways motion of the head.

(d) The orientation of the head.

(e) Contact forces on modules 3 - 5 (Trial 1).

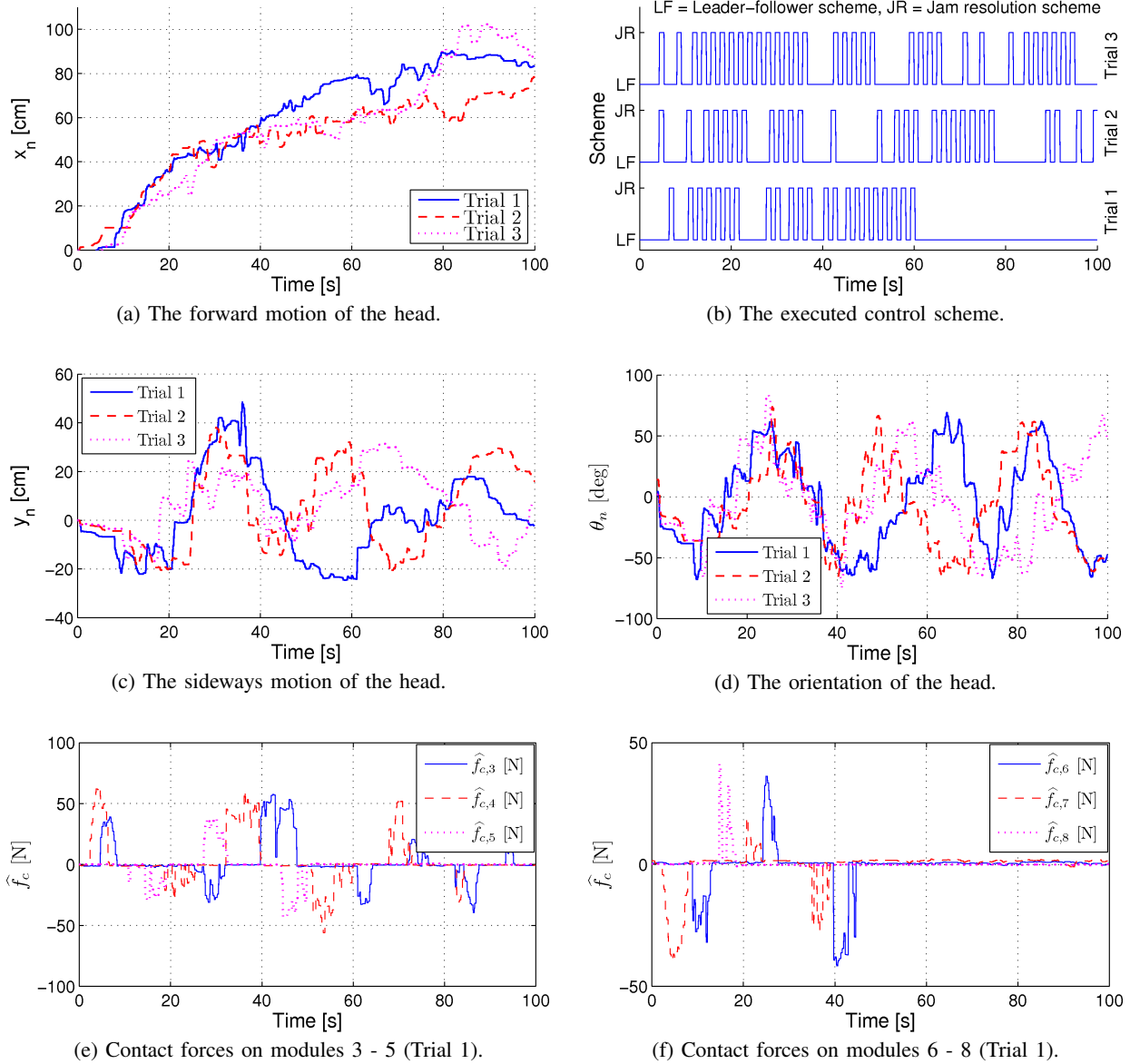(f) Contact forces on modules 6 - 8 (Trial 1).

Fig. 6. Experimental results of obstacle-aided locomotion in the first obstacle environment.

Fig. 7. The motion of the snake robot in the first obstacle environment (Trial 1).

(a) The forward motion of the head.

(b) The executed control scheme.

(c) The sideways motion of the head.

(d) The orientation of the head.

(e) Contact forces on modules 3 - 5 (Trial 1).
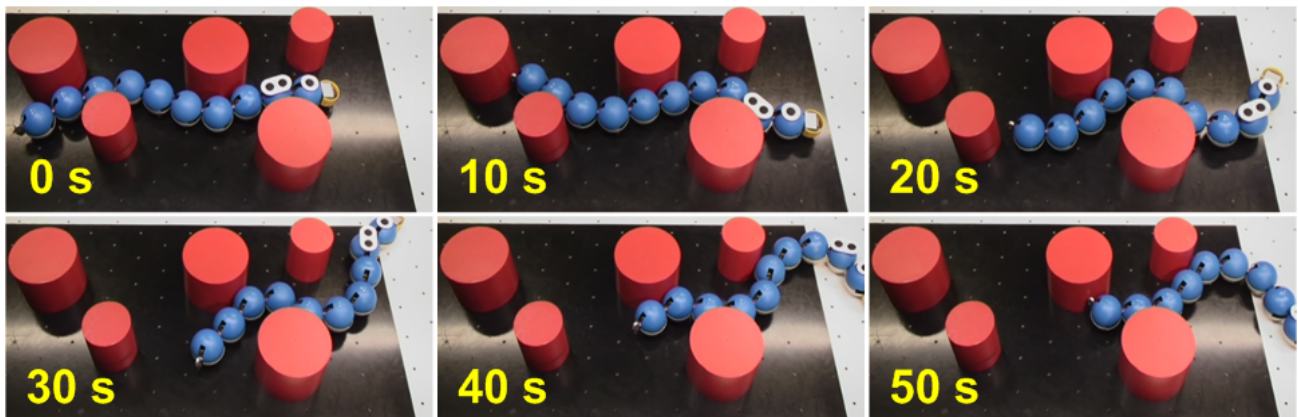
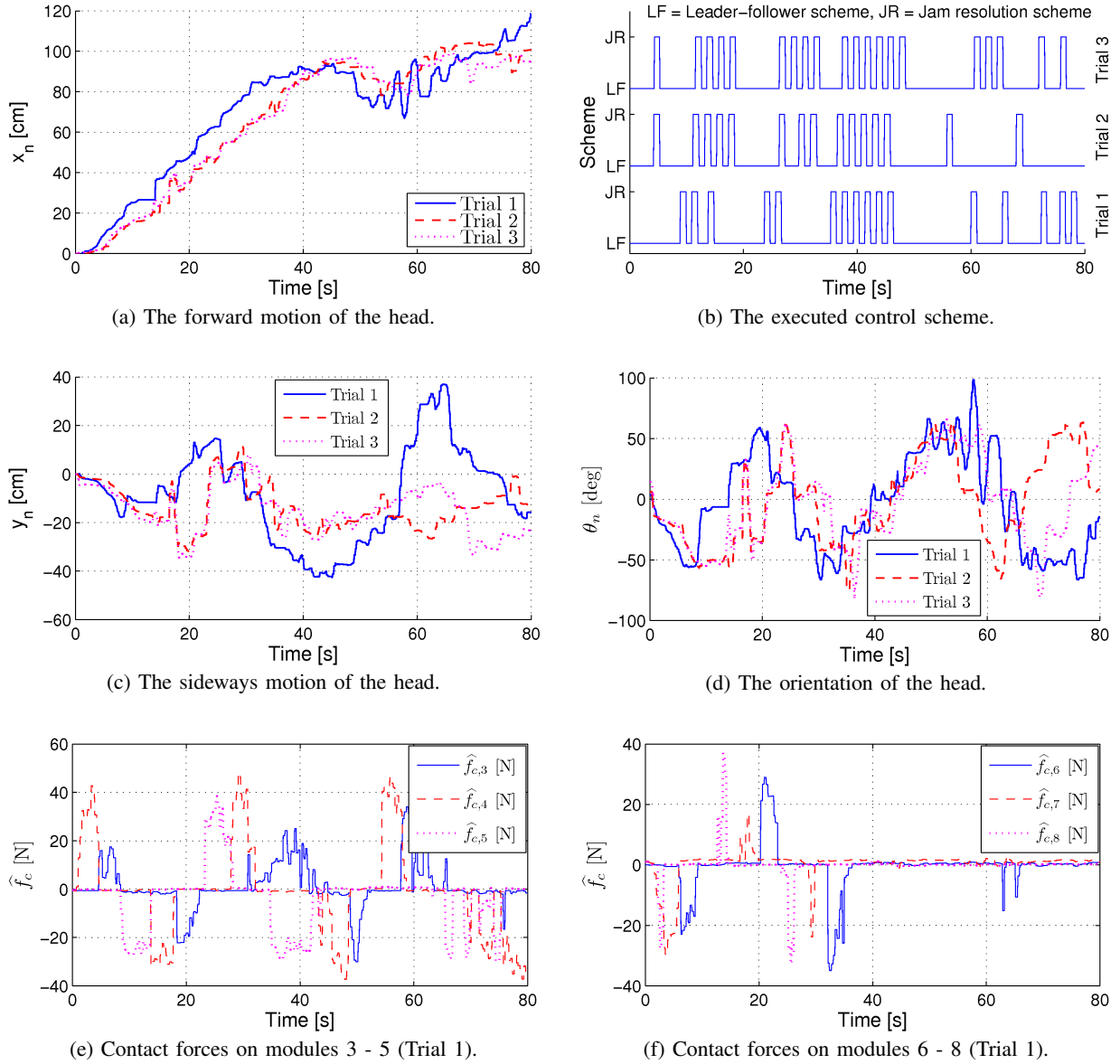(f) Contact forces on modules 6 - 8 (Trial 1).

Fig. 8. Experimental results of obstacle-aided locomotion in the second obstacle environment.
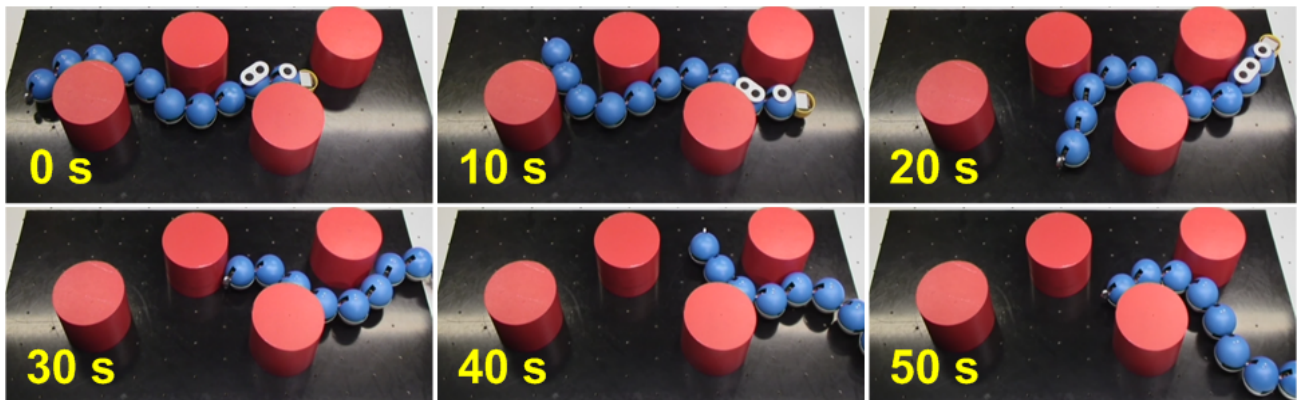
Fig. 9. The motion of the snake robot in the second obstacle environment (Trial 1).

(a) The forward motion of the head.

(b) The executed control scheme.

(c) The sideways motion of the head.

(d) The orientation of the head.

(e) Contact forces on modules 3 - 5 (Trial 1).

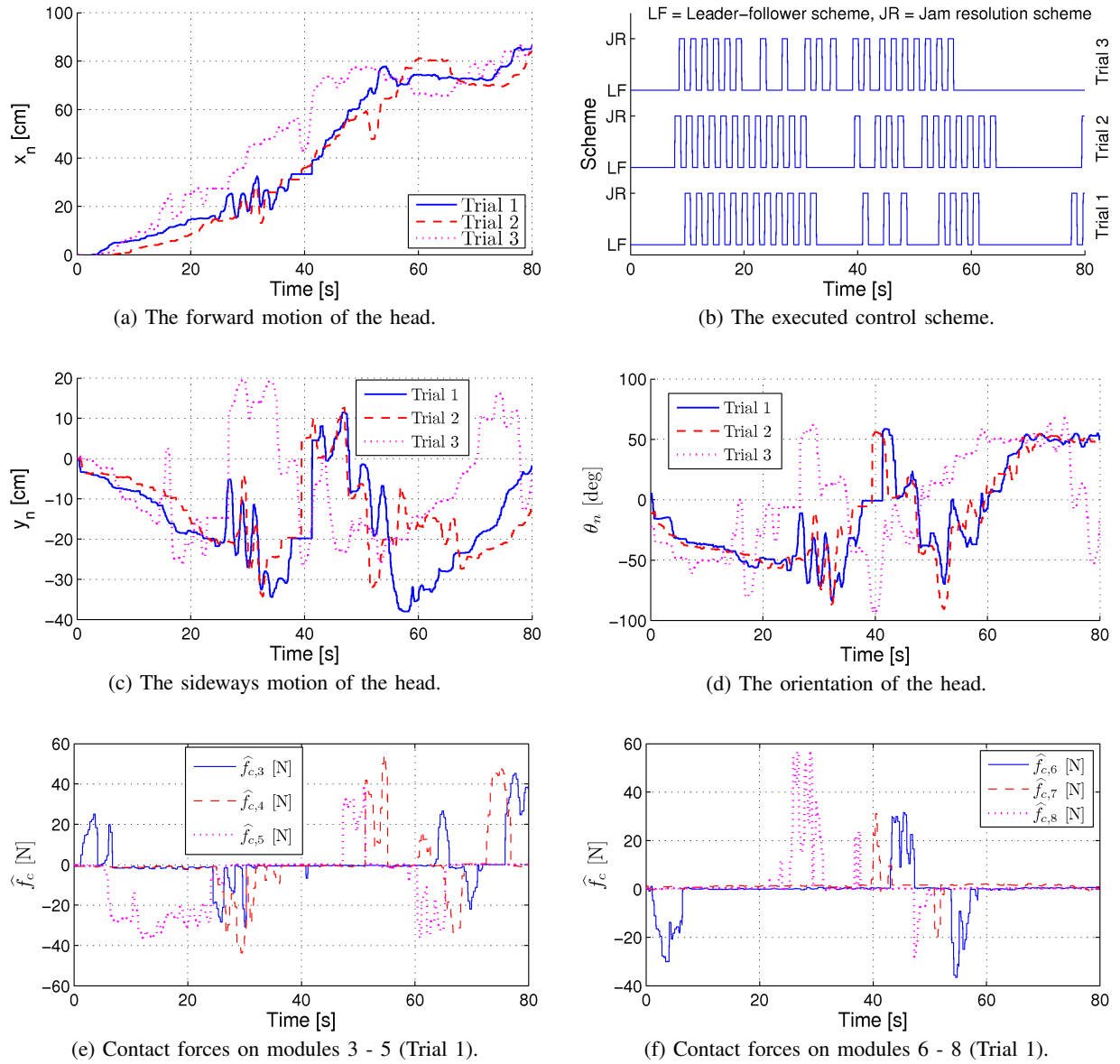(f) Contact forces on modules 6 - 8 (Trial 1).

Fig. 10. Experimental results of obstacle-aided locomotion in the third obstacle environment.
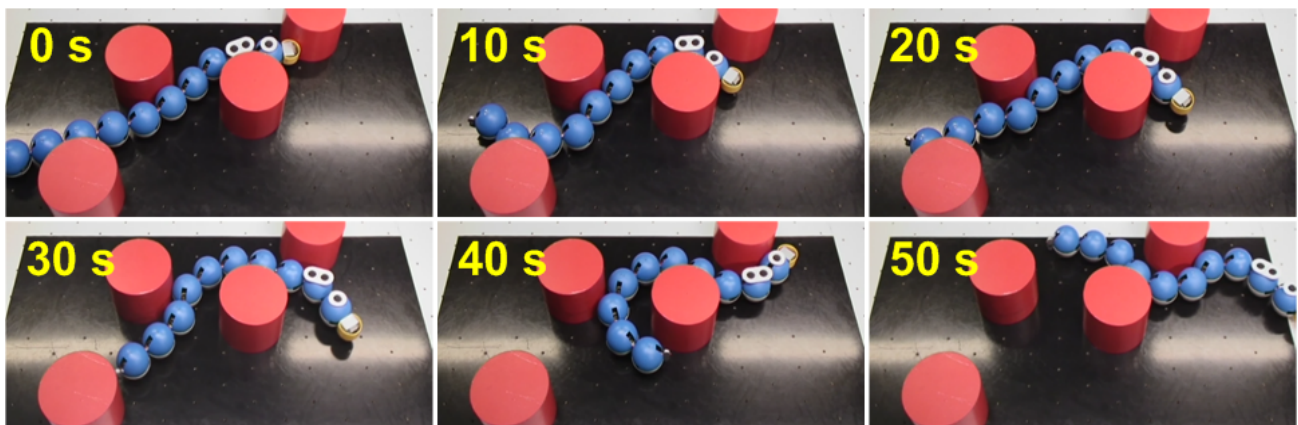

Fig. 11. The motion of the snake robot in the third obstacle environment (Trial 1).
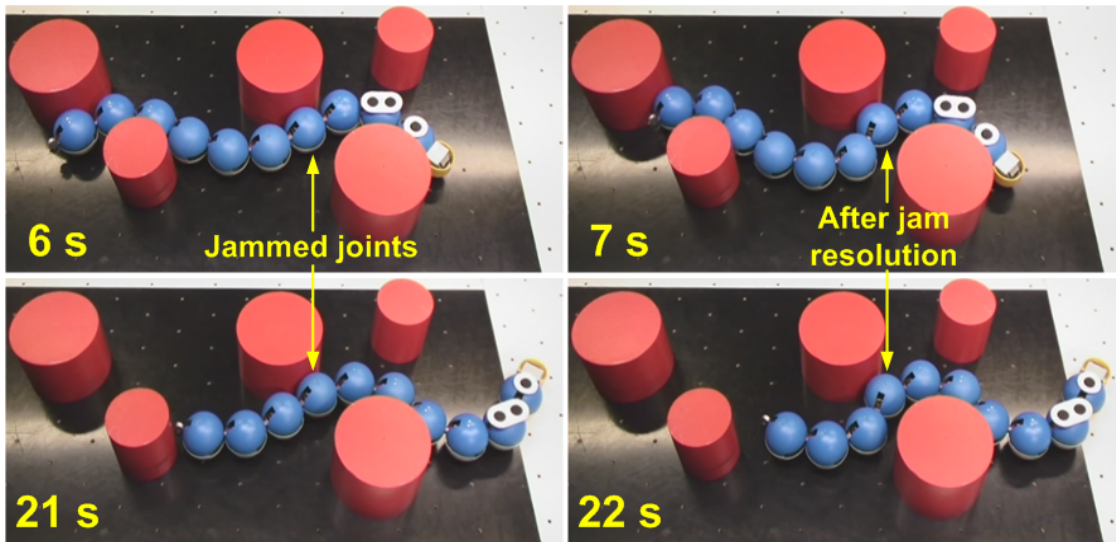
Fig. 12.   The shape of the snake robot before and after jam resolution in the first obstacle environment.

[13] Z. Y. Bayraktaroglu, "Snake-like locomotion: Experimentations with a biologically inspired wheel-less snake robot," *Mechanism and Machine Theory*, vol. 44, no. 3, pp. 591–602, 2008.

[14] Y. Shan and Y. Koren, "Design and motion planning of a mechanical snake," *IEEE Trans. Syst. Man Cyb.*, vol. 23, no. 4, pp. 1091–1100, July-August 1993.

[15] H. Date and Y. Takita, "Adaptive locomotion of a snake like robot based on curvature derivatives," in *Proc. IEEE/RSJ Int. Conf. Intelligent Robots and Systems*, San Diego, CA, USA, Oct-Nov 2007, pp. 3554–3559.

[16] A. M. Andruska and K. S. Peterson, "Control of a snake-like robot in an elastically deformable channel," *IEEE/ASME Trans. Mechatronics*, vol. 13, no. 2, pp. 219–227, april 2008.

[17] A. Kuwada, S. Wakimoto, K. Suzumori, and Y. Adomi, "Automatic pipe negotiation control for snake-like robot," in *Proc. IEEE/ASME Int. Conf. on Advanced Intelligent Mechatronics*, July 2008, pp. 558–563.

[18] P. Liljebäck, K. Y. Pettersen, Ø. Stavdahl, and J. T. Gravdahl, "Hybrid modelling and control of obstacle-aided snake robot locomotion," *IEEE Trans. Robotics*, vol. 26, no. 5, pp. 781–799, Oct 2010.

[19] R. Goebel, R. Sanfelice, and A. Teel, "Hybrid dynamical systems," *IEEE Contr. Syst. Magazine*, vol. 29, no. 2, pp. 28–93, 2009.

[20] P. Liljebäck, K. Y. Pettersen, and Ø. Stavdahl, "A snake robot with a contact force measurement system for obstacle-aided locomotion," in *Proc. IEEE Int. Conf. Robotics and Automation*, Anchorage, AK, USA, 2010, pp. 683–690.

[21] T. Lochmatter, P. Roduit, C. Cianci, N. Correll, J. Jacot, and A. Martinoli, "Swistrack - a flexible open source tracking software for multi-agent systems," in *IEEE/RSJ Int. Conf. Intelligent Robots and Systems*, 2008, pp. 4004–4010.